Cation-Anion Interactions within the Nucleic Acid Ion Atmosphere Revealed by Ion Counting

Magdalena Gebala,[†] George M. Giambașu,[‡] Jan Lipfert,[§] Namita Bisaria,[†] Steve Bonilla,[‖] Guangchao Li,[⊥] Darrin M. York,[‡] and ,Daniel Herschlag*[,†,#]

[†]Department of Biochemistry, Stanford University, Stanford, California 94305, United Sates

[‡]BioMaPS Institute for Quantitative Biology and Department of Chemistry and Chemical Biology, Rutgers University, Piscataway, New Jersey 08854, United States

[§]Department of Physics, Nanosystems Initiative Munich, and Center for Nanoscience, Ludwig Maximilian University of Munich, 80799 Munich, Germany

[‖]Department of Chemical Engineering, Stanford University, Stanford, California 94305, United States

[⊥]School of Earth, Energy and Environment Sciences, Stanford, California 94305, United States

[#]Department of Chemistry, Stanford University, Stanford, California 94305, United States

*Corresponding author: herschla@stanford.edu

Table of Contents

Overview of the Supplementary Information

In this Supporting Information, we describe controls to determine dependence and accuracy of the ion counting method on DNA concentration (Figure S1); to establish complete equilibration between DNA-containing samples and the buffer (Figure S2 and S3); to determine the linear range and precision of the spectrometers (Figure S4); to validate that Inductively Coupled Plasma Atomic Emission Spectroscopy (ICP AES) and Inductively Coupled Plasma Mass Spectroscopy (ICP MS) can be used interchangeable to analyze Na, P, As (Table S1); and to determine the effect of sample dilution on measurements precision (Table S2).

We provide plots of the number of accumulated cations around a 24 bp DNA (*24bp*) as a function of the anion identify over range of concentrations (Figure S5); scatter plots of k_{fold} versus k_{unfold} rate constants and the bulk equilibrium constant of P4-P6 RNA folding obtained through smFRET measurements (Figure S6 and S7 and Table S7); a plot of the equilibrium constant of P4-P6 RNA folding as a function of the number of accumulated cations determined through the ion counting experiments (Figure S8); a comparison between the number of accumulated cations and mean activity coefficients of given electrolytes at bulk ion concentrations of 10 mM, 100 mM, and 200 mM (Figure S9); and plots presenting the dependences of ion counting results on solution activity (Figure S10). The results are consistent with observations in the main text and support the conclusions described therein.

We also present a comparison of our results to previous experimental data (Table S6).

Dependence and accuracy of the ion counting method on DNA concentration

The ion preferential interaction coefficients –i.e., the number of associated ions around *24bp* is determined according to:

$$\Gamma_i = \frac{c_{ion}^{DNA} - c_{ion}^{bulk}}{c_{DNA}} \tag{S1}$$

Ion concentration in the DNA-containing sample and the bulk solution (i.e., corresponding flow through), as well DNA concentrations, were measured by ICP AES and ICP MS, as described in the main text. We noticed that to ensure high accuracy of the ion counting method, the percentage change in concentrations between ions in the DNA-containing sample and the bulk solution (the nominator of the above equation) should be above a propagated instrument error that falls within 5%. The propagated instrument error was determined by monitoring a quality control sample (QC) assayed every ten analyzed samples. Nonlinearities in standard curves are consistent with the known instrument limitations[1] and these concentrations ranges were not used in our analyses.

For these reasons, the DNA concentrations of samples were adjusted to ensure, that the ion concentration difference was sufficiently large and, over a range of sample concentrations, that the number of associated ions was independent of the DNA concentration (Figure S1).

Equilibration between the DNA-containing sample and the buffer

To determine the number buffer exchange rounds required to ensure equilibration between the DNA-containing sample and the buffer, we monitored the ion constituents of the flow-through through a series of equilibration rounds (Figure S2). For low ion and DNA concentrations, samples were equilibrated after

two buffer exchange rounds. Higher concentrations of salt and DNA required more buffer exchanges. Based on these results we carried out eight rounds of the buffer exchange for all samples, regardless of salt or DNA concentration.

We also independently demonstrated that equilibration was achieved by comparing the ion content of the last flow-through (after the eighth round of the buffer exchange) with the starting solution (Figure S3).

Spectrometer linear range

We determined the linear range and precision of the OES and MS spectrometer for each element. A concentration series of the element under study (1-200 µM) was prepared by sequential dilutions of a stock (made with a high standard from SPEX CetriPrep). Plotting the expected concentrations of the series versus the measured values gave a standard curve for each element (Figure S4). The deviation in repeated standard curves gave the systematic precision of the spectrometers.

Correlations between ion preferential interaction coefficients and solution activity coefficients and activity.

The activity coefficient of a given monovalent electrolyte solution is expressed by a mean value that is defined as:

$$\gamma_\pm = \sqrt{\gamma_+ \cdot \gamma_-} \tag{S2}$$

where $\gamma_\pm$ is the mean activity coefficient and γ_+ and γ_- are activity coefficient on a cation and an anion, respectively. Individual activity coefficients of the cation and anion cannot be measured. Instead the mean activity coefficient of a given salt is experimentally determined.

Activity coefficients are a complex amalgam of short and long range correlations between salt components that reflect properties of the ions and the solvent.[2-4] At infinite dilutions, where electrolytes properties are approaching ideal behavior, the activity coefficient is equal 1. Any deviations from this reference state indicate interactions or correlations between solution particles: ions and water.[2,3,5] It has been noticed, that electrolyte solutions with more predominant cation-anion correlations show lower activity coefficients at high concentrations compare to electrolytes with little or no short-range ion correlations.[2,3] The simplest and most often considered factor that contributes to lowering activity coefficients of salt solutions is the formation of ion pairs.[2,3] The thermodynamic effect of the ion pair formation is a removal of a certain number of free ions from solutions. The effective concentration of solutions i.e., activity is related to concentrations by the activity coefficient:

$$a_\pm = \gamma_\pm \cdot m_{salt} \tag{S3}$$

where $a_\pm$ is the activity, m_{salt} is molality of salt solution.

In Figure S10 experimentally determined cation preferential coefficients (Γ_+) for NaX, RbX and CsX salts are compared to activities of given salts. These activates are estimated following eq S3 and using $\gamma_\pm$ provided in ref [6].

In Figure S10, the value of Γ_+ for salts with larger activity coefficient effects and thus lower activity are shifted more to the left with respect to x-axis (activity). Representing Γ_+ as a function of activates instead of total concentrations allows comparison of different salts accounting at least to some extent for differential availability of solution cations for screening. A simple expectation would be that by using activities and thus normalizing all salt solutions to the same effective concentration, all Γ_+ values would

follow the same dependence. However Figure S10 demonstrates that this is not the case, indicating that cation-anion correlations affect not only properties of the bulk solution but have additional effects within the ion atmosphere.

Poisson Boltzmann estimates of ion preferential interaction coefficients

The preferential coefficients of ions i of valence z_i associated with the DNA was computed by integrating the excess ion density [7-9]:

$$\Gamma_i = \rho_{b,i} \int (\lambda(r)e^{-z_i e\varphi(r)/kT} - 1)dr = \rho_{b,i} \int \lambda(r)e^{-z_i e\varphi(r)/kT}dr - \rho_{b,i} \int dr \qquad (S4)$$

where $\rho_{b,i}$ is the bulk ion density, $\lambda(r)$ is an accessibility factor that defines the region in space that is accessible to ions (where $\lambda(r) = 1$ and $\lambda(r) = 0$ for the solvent-excluded region –i.e., inside the macromolecule)[10], e is the elementary charge, $\varphi(r)$ is the electrostatic potential, k is the Boltzmann constant, and T is the temperature.

Ion counting experiments are carried out volumetrically; thus PB calculations should match these experimental conditions. This match is achieved by defining the integration volume (eq S4) as the entire volume of a simulation box; one that contains the dsDNA molecules (box 1 in Figure S12A) and one of the same volume that represents the bulk solution (box 2 in Figure S12A).

In previous PB calculations[9,11] the volume of the bulk solution was defined as equal to the accessible volume in box 1; i.e., the difference between the volume of the simulation box and the volume of a dsDNA molecule or other electrolyte (see Figure S12B). This approach implies equal amount of solvent in both boxes and leads to an overestimate of the predicted number of ions (both cations and anions) relative to the experimental ion counting values. For this reason we did not use this approach for the PB calculations herein (Figure S12A).

In addition, we tested the effect of the internal dielectric constant of the DNA (ε_{DNA}) and the ion size (R_{ion}) on PB predictions of the ion preferential coefficients (Γ_i). We carried out calculations for ε_{DNA} equal 2, 4 and 10 with R_{ion} equal 2 Å and predicted Γ_i are identical within 0.5% relative error (Figure S14).

The PB theory treats ions as point charges and thus, in principle, it does not account for differences in the ion size. Nevertheless, in PB calculations of the preferential interaction coefficients, there is a size term for the distance of closest approach (a = $R_{DNA} + R_{ion}$, where R_{ion} is the ion size and R_{DNA} is the dsDNA radius).[12,13] The distance of closest approach defines the excluded volume of the dsDNA that it is known to effect NLPB calculations of Γ_i only at relatively high salt concentrations. We carried out PB predictions for R_{ion} equal 2 Å and 4 Å (Figure S15). We observed that PB predictions with R_{ion} of 2 Å give approximately 2 ions less at high salt concentrations (500 mM).

Supplementary Figures:
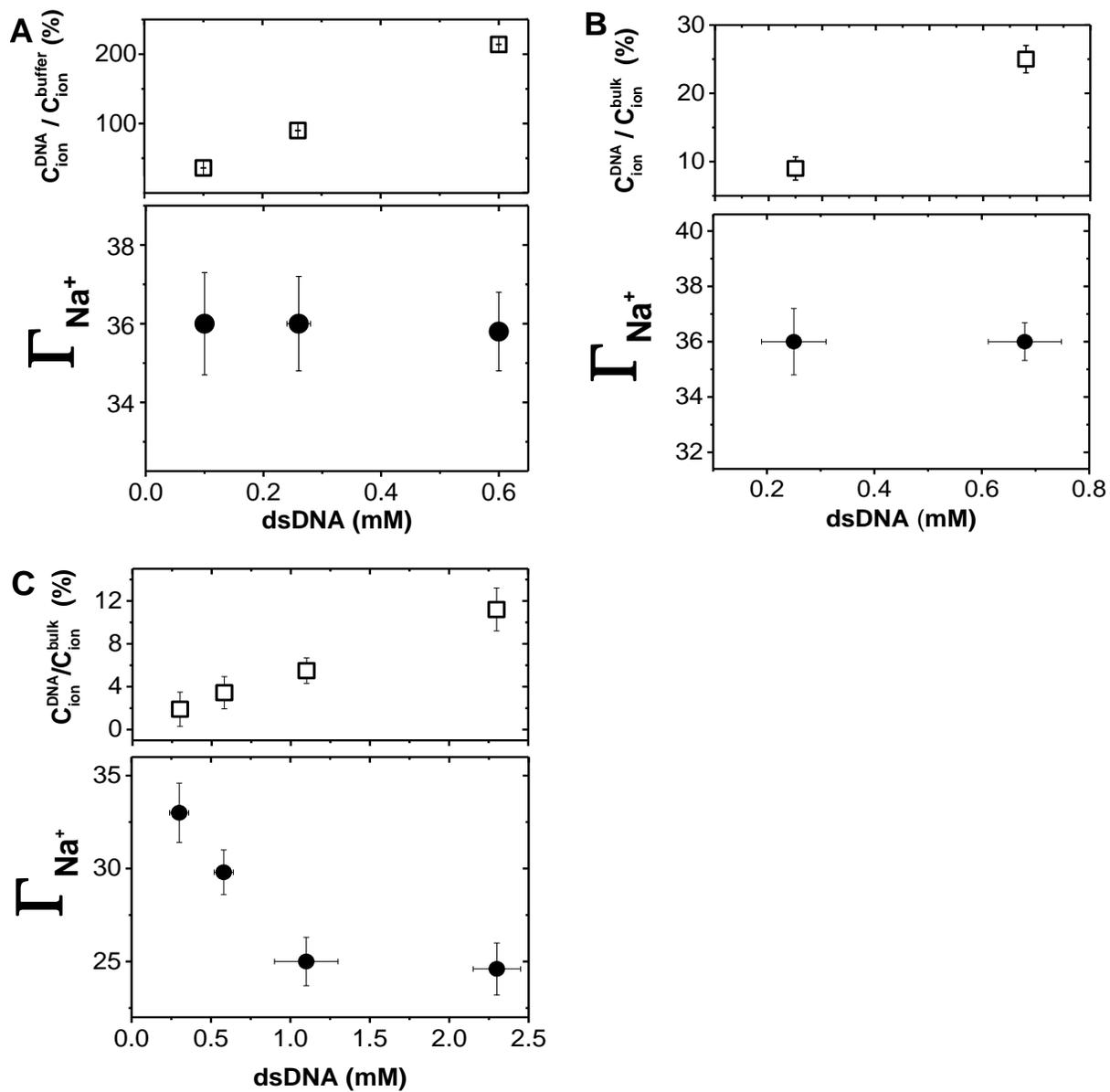
Figure S1. Dependence of the number of associated cations and the ion counting precision on the dsDNA concentration determined with 10 mM (A), 100 mM (B), and 500 mM (C) NaCl.
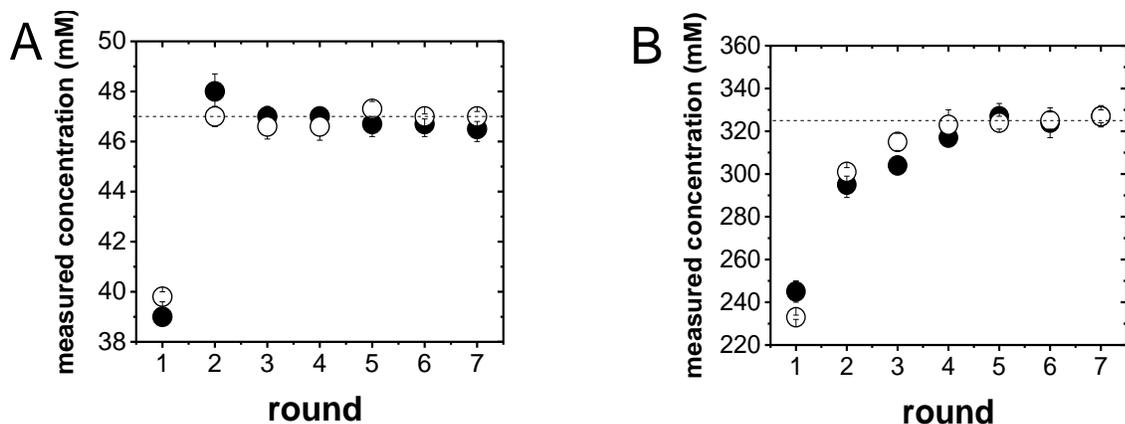
Figure S2. Equilibrium between the DNA-containing samples and the buffer is achieved by buffer equilibration. Plots show the ion content of the flow-thought measured after each equilibration round for: (A) 46 mM Na^+ (●) or 46 mM Br^- (○) with 0.4 mM *24bp* and (B) 325 mM Na^+ (●) or 325 mM Br^- (○) with 1.0 mM *24bp*.
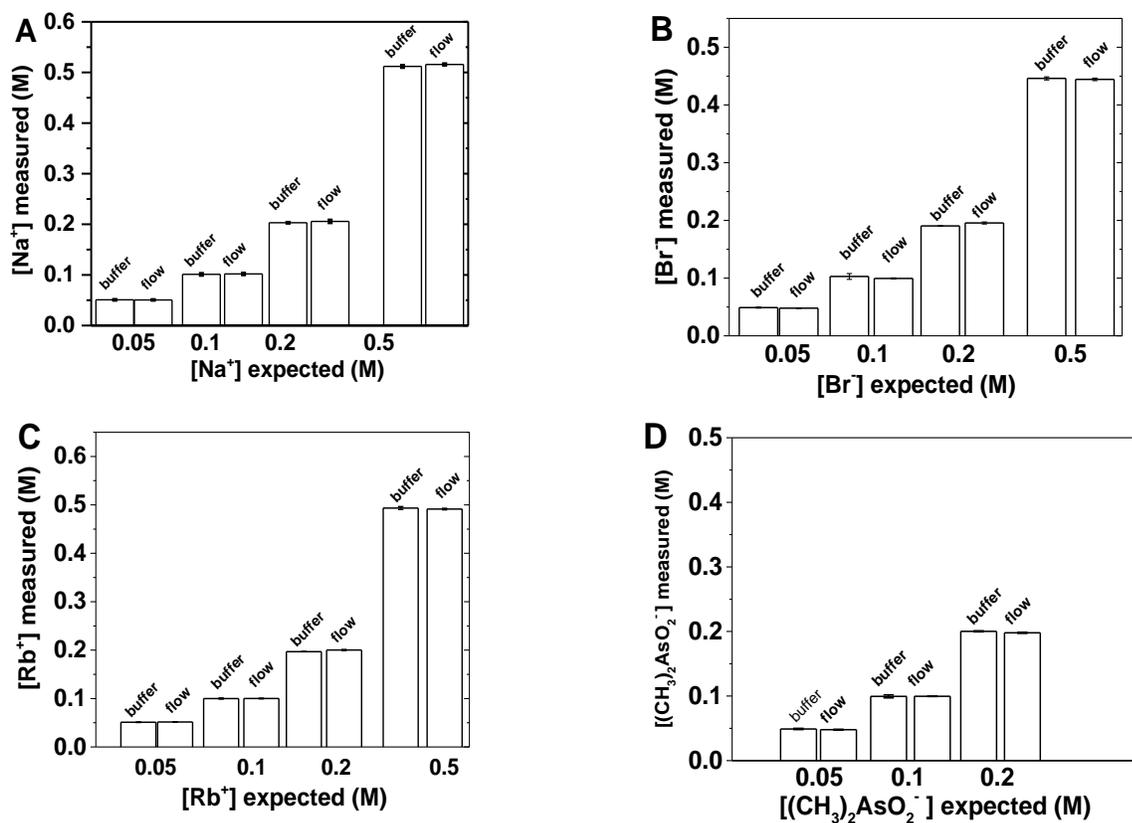
Figure S3. Equilibrium between the DNA-containing samples and the buffer is achieved by buffer equilibration. Plots show the ion constituents of the buffer and the flow-thought measured after the eighth round of buffer equilibration for NaBr: Na^+ (A), Br^- (B), and RbCacodylate: Rb^+ (C), and $As(CH_3)_2O_2^-$ (D) over a wide range of salt concentrations (0.05 - 0.5 M).
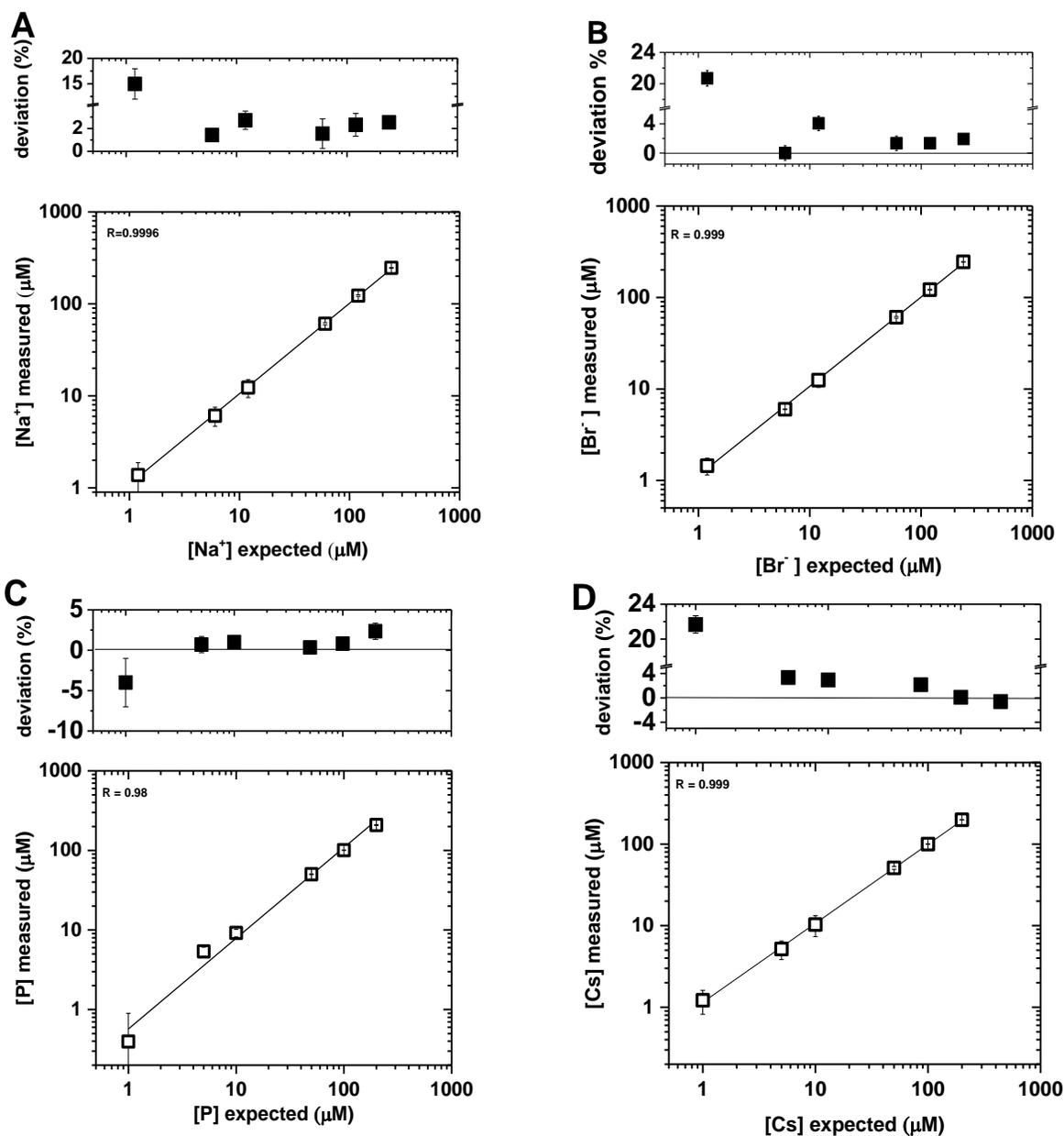
Figure S4. Standard curves for sodium (A), bromide (B), phosphorus (C) and cesium (D). The mean values of multiple AES measurements (greater than triplicates), in terms of the relative deviation from the expected values, are plotted above the main graphs; the error bars represent the statistic error around the mean and are used to estimate the precision of the AES spectrometer. Concentrations at which the measurement (a range of values bracketed by the error around the mean) departs less than 5% from the expectation are considered within the linear range.
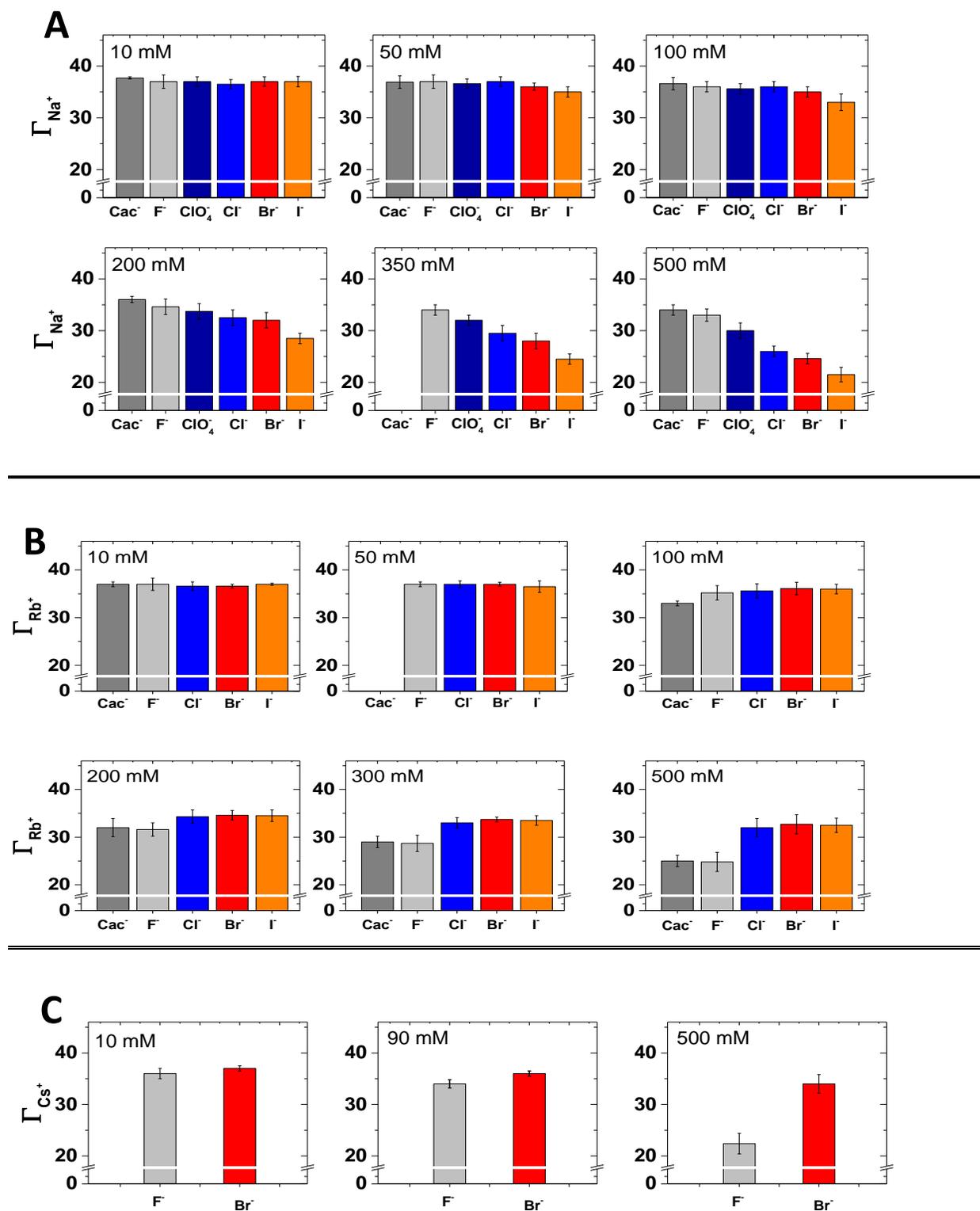
Figure S5. The number of accumulated cations around *24bp* over a range of concentrations of Na^+ (A), Rb^+ (B) and Cs^+ (C) in the presence of the specified anions. Each data point is the average of 3-5 determinations and error bars represent standard deviations.
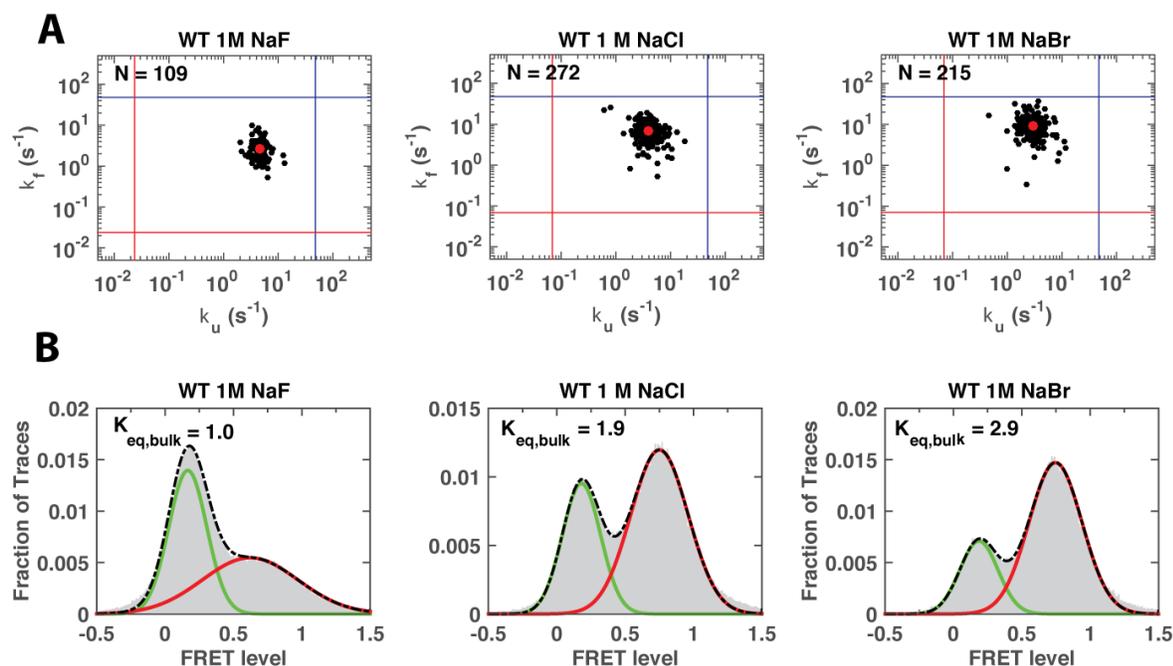
Figure S6. smFRET data for P4-P6 RNA in sodium salts. A) Plot of fitted values of k_{fold} versus k_{unfold} for each molecule. Blue lines indicate the camera frame rate and red lines indicate the average lifetime of the molecules. The red dot indicates mean folding and unfolding rate constants. TIRF measurements were taken at 50 frames per second (see Methods). The number of individual molecules is provided in upper-left corner of each plot. B) Distribution of FRET intensity. FRET intensity is defined as the intensity of each molecule in the acceptor channel divided by the intensity found in both the donor and the acceptor channels. The FRET intensity distribution was fit with a two-Gaussian model representing the fraction of total time the population of molecules spends in each state. The equilibrium constant ($K_{eq,bulk}$) was determined from the ratio of the fraction of molecules that are in the high FRET peak (red) versus low FRET peak (green). The apparent FRET values range from <0 to >1 as a result of varying background and noise contributions. Conditions: 50 mM Na-MOPS, pH 8.0, 1 M NaX, at 23 °C.
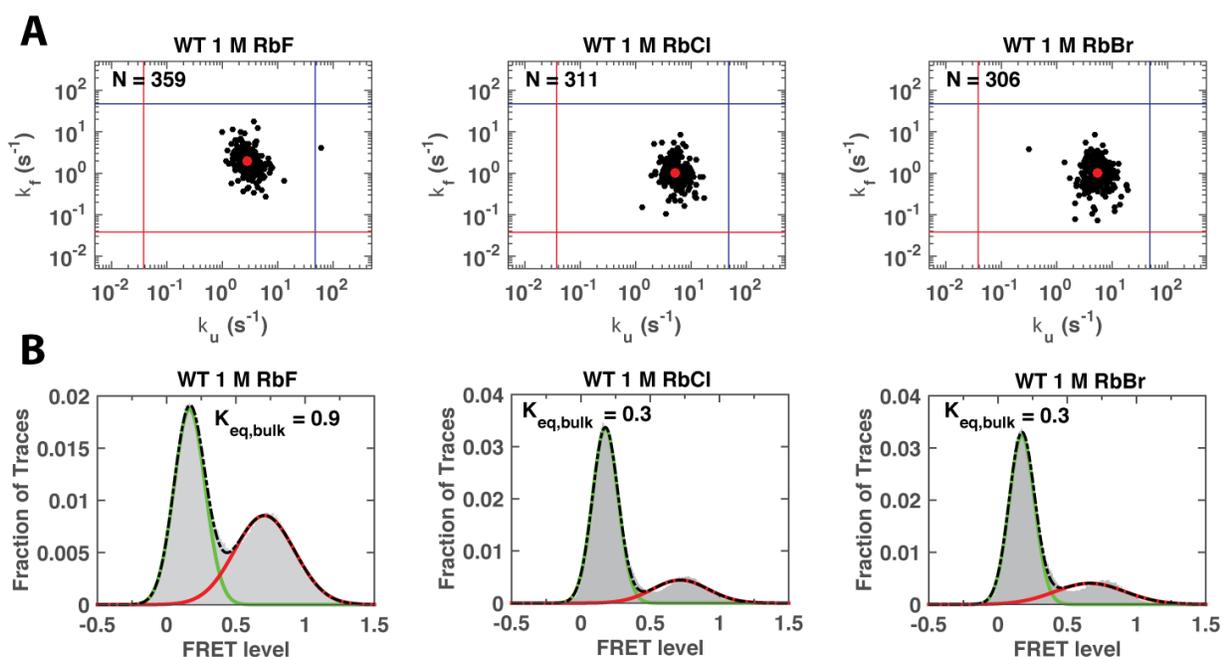
Figure S7. smFRET data for P4-P6 RNA in rubidium salts. A) Plot of fitted values of k_{fold} versus k_{unfold} for each molecule. Blue lines indicate the camera frame rate and red lines indicate the average lifetime of the molecules. The red dot indicates mean folding and unfolding rate constants. TIRF measurements were taken at 50 frames per second (see Methods). The number of individual molecules is provided in upper-left corner of each plot. B) Distribution of FRET intensity. FRET intensity is defined as the intensity of each molecule in the acceptor channel divided by the intensity found in both the donor and the acceptor channels. The FRET intensity distribution was fit with a two-Gaussian model representing the fraction of total time the population of molecules spends in each state. The equilibrium constant ($K_{eq,bulk}$) was determined from the ratio of the fraction of molecules that are in the high FRET peak (red) versus low FRET peak (green). The apparent FRET values range from <0 to >1 as a result of varying background and noise contributions. Conditions: 50 mM Na-MOPS, pH 8.0, 1 M RbX, at 23 °C.
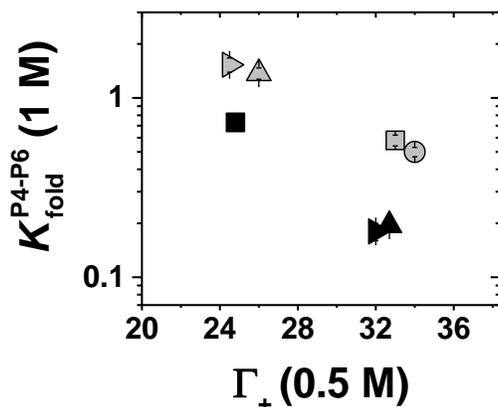
Figure S8. Plot of P4-P6 RNA folding equilibria versus the cation preferential interaction coefficient (Γ_+) with *24bp* for the same cation/anion pair. Equilibrium constant of P4-P6 folding at 1 M NaX (grey) or RbX (black) with the following symbols for anions F⁻ (■), Cl⁻ (▲), and Br⁻(▶). Error bars correspond to the bootstrap-estimated 95% confidence intervals (SD = 2σ bootstrap)
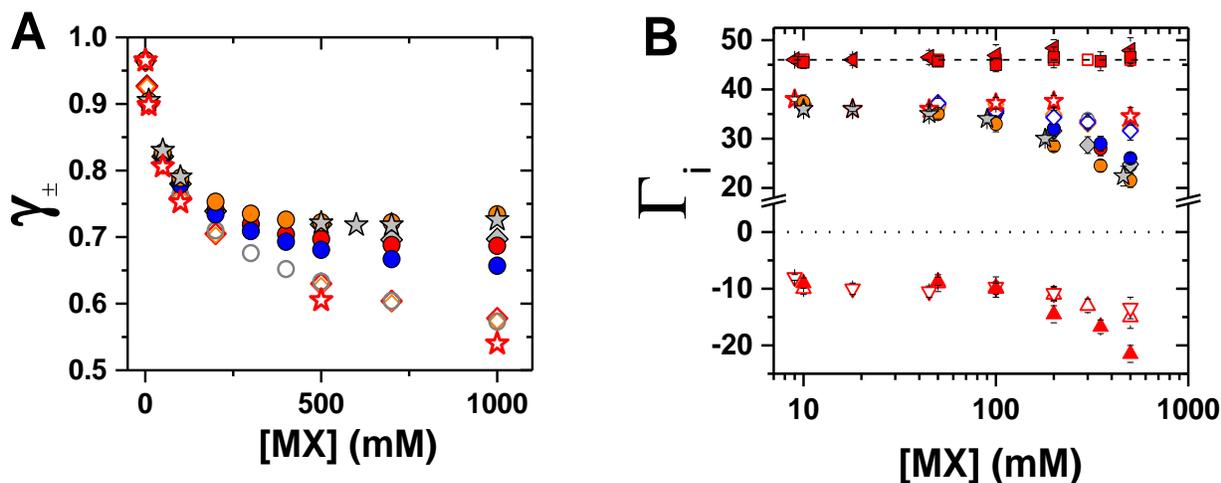
Figure S9. Relationship between mean activity coefficients of monovalent salt solutions ($\gamma_\pm$) and the ion excess (Γ_i) around *24bp*. Dependence of the mean activity coefficient (A) and the number of associated ions (B) on salt concentration. Solutions cluster in two groups: low activity coefficient (open symbols): NaF (grey ○), RbCl (blue ◊), RbBr (red ◊), RbI (orange ◊), CsBr (red stars) and high activity coefficient (closed symbols): NaCl (blue ●), NaBr (red ●) and RbF (grey ◆), CsF (grey stars). Activity coefficients in (A) are from ref [6]. In (B), each data point is the average of 3-5 determinations.

S12
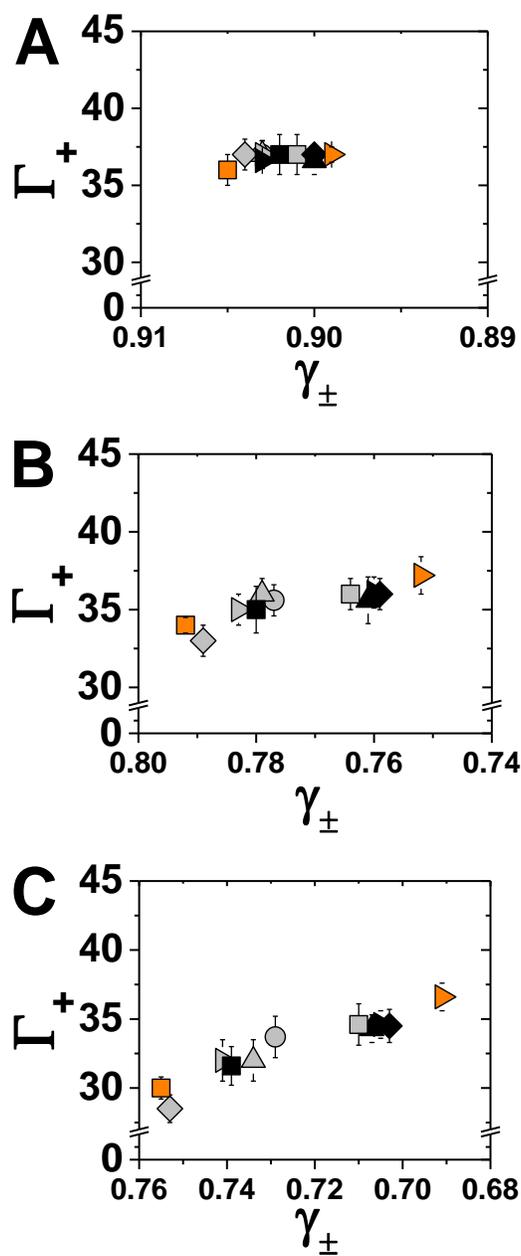
Figure S10. Dependence of cation preferential interaction coefficients (Γ_+) on the mean activity coefficient for a series of electrolyte solutions. The number of cations associated with *24bp* DNA ($\gamma_\pm$) as a function of mean activity coefficients at 10 mM (A), 100 mM (B) and 200 mM (C) bulk ion concentration. NaX salts are represented in grey, RbX salts in black, and CsX salts in orange. Salts that share the same anion are represented by the same symbols: NaF, RbF, and CsF (■: grey, black, orange, respectively); NaCl, RbCl (▲: grey, black); NaBr, RbBr, and CsBr (▶: grey, black, orange, respectively); and NaI and RbI (♦: grey, black).
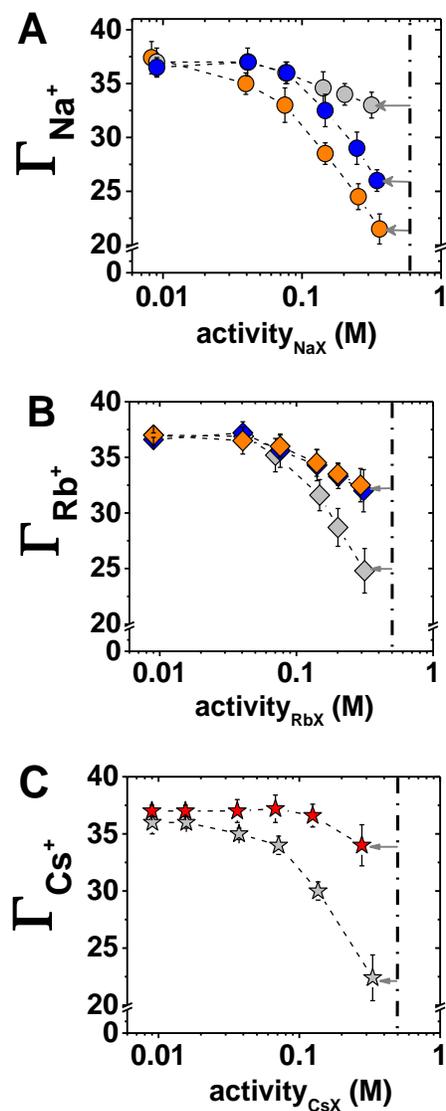
Figure S11. Cation preferential interaction coefficients as a function of the activity of salt solutions. Sodium (A), rubidium (B), and Cs (C) preferential interaction coefficients in the presence of F⁻ (grey), Cl⁻ (blue), Br⁻ (red, only in (C)) and I⁻ (orange). Salts with larger activity coefficient effects (i.e., lower activity coefficients) have lower effective concentrations. Grey arrows and the vertical dash-dotted line at 0.5 M are provided to visualize this difference. Dashed lines connecting data points are provided as guides.

A

1   2

$\Gamma_+ = 8 \quad \Gamma_- = -3$

B

1   2

$\Gamma_+ = 10 \quad \Gamma_- = -1$

Calculated
preferential interaction coefficients

legend:

| total volume of a sample | negatively charged dsDNA | cylinder representing dsDNA volume | cation anion |
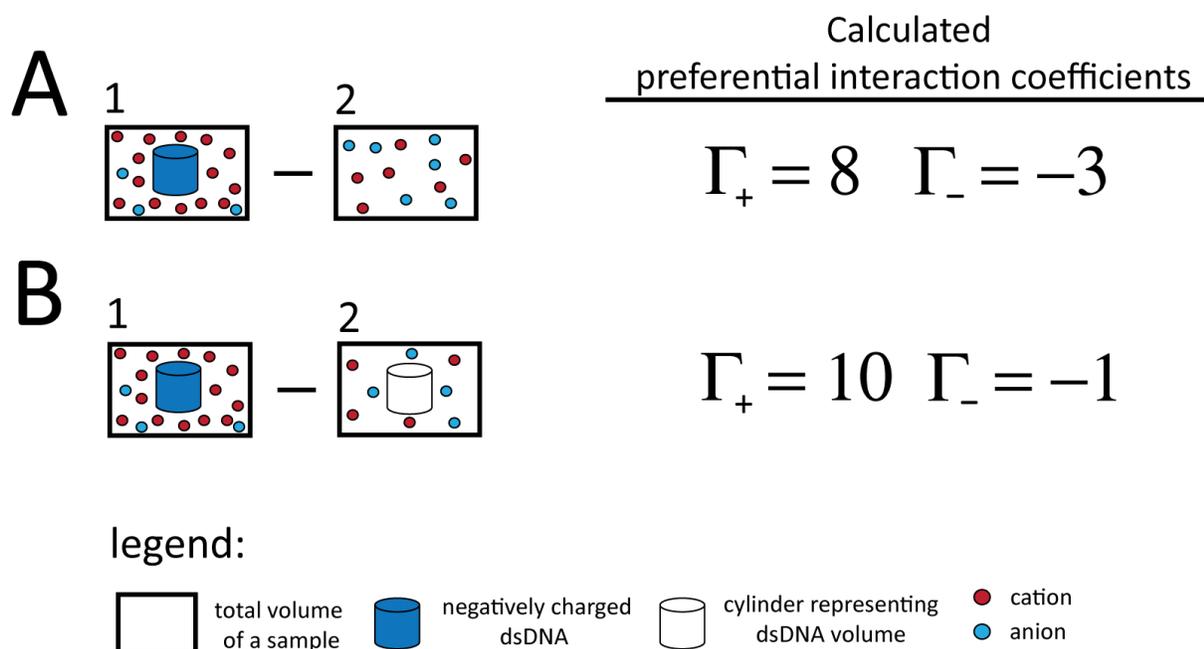
$$\Gamma_{ion} = N_{ion}(1) - N_{ion}(2)$$

Figure S12. Schematic representation of a PB calculation of preferential interaction coefficients. A) PB calculations carried out to reproduces volumetric experimental conditions. Box 1 contains the negatively charged dsDNA molecules, excess of cations and a deficit of anions compared to the reference state (i.e., the bulk solution (box 2)). Box 2 is simply the salt solution and contains an equal number of cations and anions. The preferential interaction coefficient for cations and anions is defined as the difference between the number of ions in box 1 and box 2. Note that the volume of box 2 that is accessible to solvent is larger than that of box 1. B) PB calculations carried out with equal accessible volumes in both simulation boxes. The content of box 1 as described above. Box 2 contains a neutral 'dummy' dsDNA of the same volume as the dsDNA in box 1 and a solvent with an equal concentration (but not number) of cations and anions as in box 2 of panel (A). Placing the neutral dsDNA in box 2 implies equal accessible volumes in both boxes. Calculation of preferential interaction coefficients following this scheme lead to an overestimate of predicted number of ions (both cations and anions) relative to the experimental ion counting values (see Figure S13B).
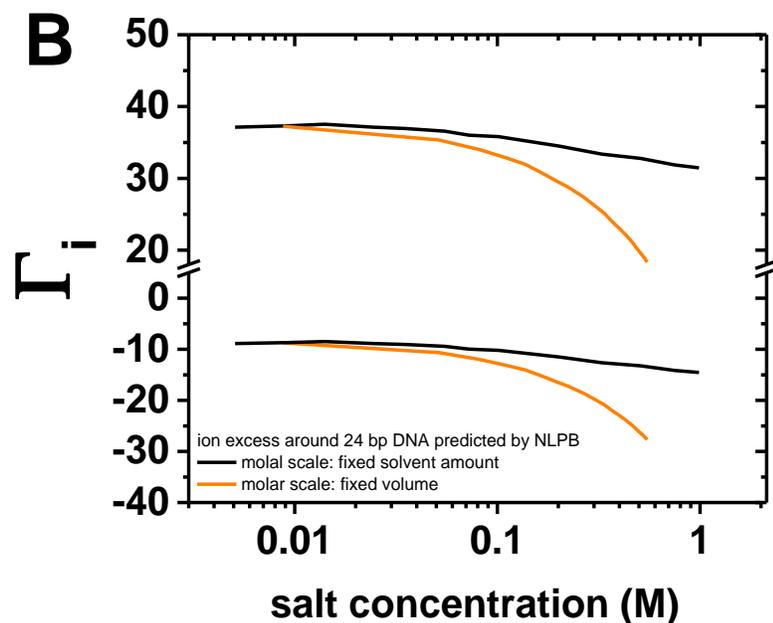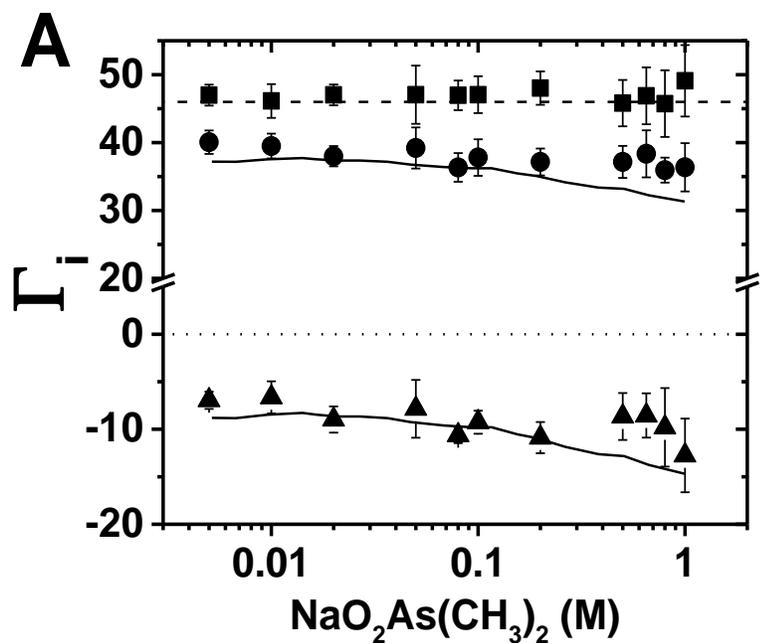
Figure S13. Comparison of PB predictions for preferential interaction coefficients (Γ). A) $NaO_2As(CH_3)_2$ preferential interaction coefficients (symbols) and PB prediction estimated in molal scale, according the method outlined in Figure S12, panel (B), and as provided by Bai et al. [9] B) Comparison of PB prediction for preferential interaction coefficients carried out in molal scale (black solid line) and molar scare (orange solid line), according the method outlined in Figure S12; panel (A, Figure S12) represents calculations using molar scale, panel (B, Figure S12) represents calculations using molal scale.
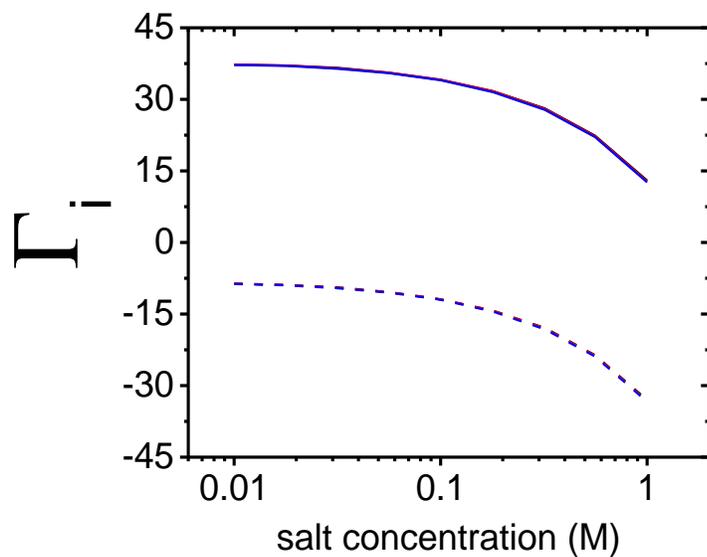
Figure S14. Comparison of PB predictions for preferential interaction coefficients (Γ_i) with various ε_{DNA}. ε_{DNA} of 2 in black, ε_{DNA} of 4 in red and ε_{DNA} of 10 in blue. PB predictions of Γ_+ are shown by the solid line and PB predictions of Γ_+ are shown by the dashed line.
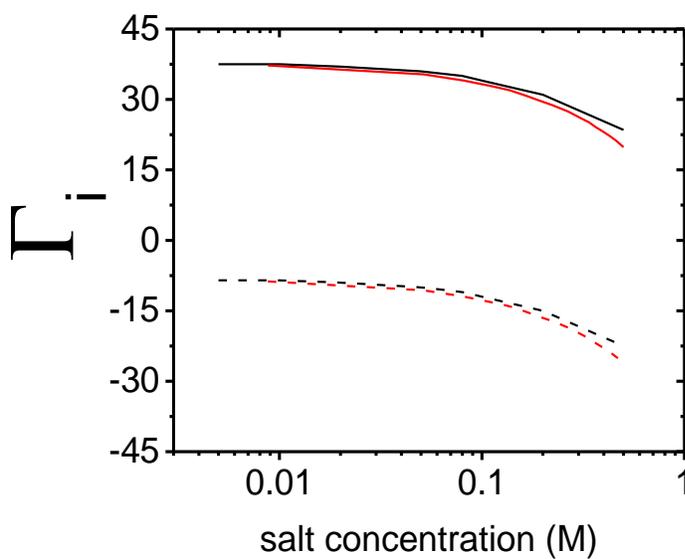
Figure S15. Comparison of PB predictions for preferential interaction coefficients (Γ_i) with various ion radii (R_{ion}). R_{ion} of 2 Å in black, R_{ion} of 4 Å in red. PB predictions of Γ_+ are shown by the solid line and PB predictions of Γ_+ are shown by the dashed line.
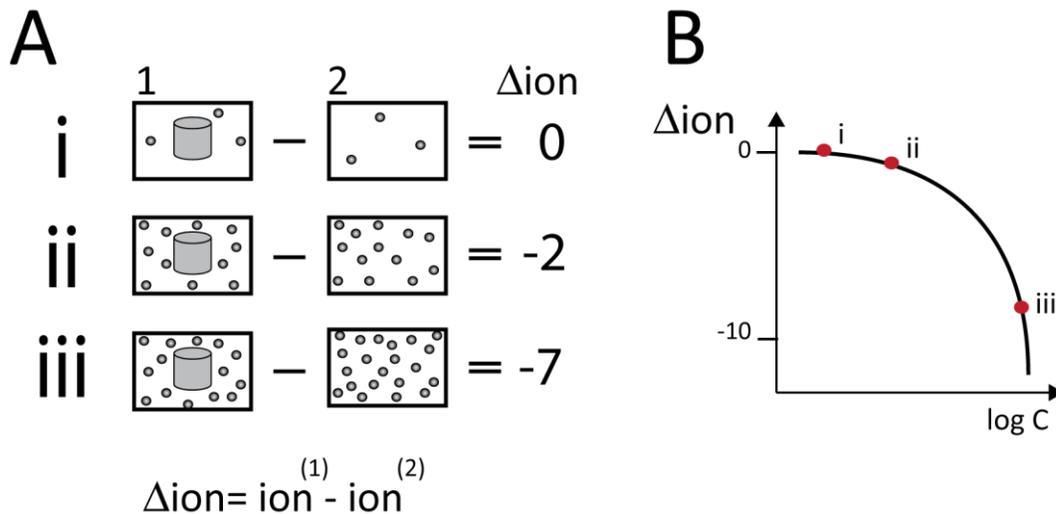
Figure S16. Schematic representation of the excluded volume effect on ion counts. A) Box 1 contains a neutral 'dummy' dsDNA molecule and a certain number of ions corresponding to a given salt concentration that increases in panels i, ii, and ii. This neutral DNA allows us to evaluate excluded volume effects and separate them from in atmosphere effects. Box 2 represents the reference state that is the bulk solution. The size of boxes is the same so that the total volumes are the same; however, the accessible volumes in the two boxes are not equal. The accessible volume of box 1 is lowered by the presence of dsDNA, which excludes solvent from the space that it occupies. We present three bulk concentration regimes: i) low, ii) moderate, and iii) high. At low concentrations, the number of ions in both boxes is the same and therefore Δion (i.e. the difference in the number of ions between box 1 and box 2, which represents the number of excluded ions) is essentially equal to zero. At moderate and high concentrations, there are fewer ions in box 1 compared to box 2 due to the presence of the dsDNA. This leads to negative values of Δion. B) The number of excluded ions from part (A) plotted as a function of the bulk ion concentration.

Table S1. Comparison of element analysis between ICP OES and ICP MS

element	Measured concentration (µM)	
	ICP OES	ICP MS
Na	101 ± 1.00	100 ± 1.00
	18.4 ± 0.30	18.0 ± 0.50
P	98.0 ± 1.00	97.0± 0.50
	24.0 ± 0.20	24.0 ± 0.15
As	110 ± 1.00	110 ± 0.50
	12.0 ± 0.50	12.0 ± 1.00

Table S2. Effect of dilutions on precision of ion counting measurements

dilution factor	$[Na^+]$ 40 mM		$[Cs^+]$ 40 mM		$[Br^-]$ 40 mM	
	Measured concentration (µM)	$[Na^+]$ (mM) [a]	Measured concentration (µM)	$[Cs^+]$ (mM)[a]	Measured concentration (µM)	$[Br^-]$ (mM) [a]
501	79.0 ± 0.10	39.6 ± 0.05	80.2 ± 0.03	40.2 ± 0.01	78.0± 0.05	39.1 ± 0.02
1001	41.5 ± 0.10	41.5 ± 0.10	41.06 ± 0.05	41.06 ± 0.05	39.3± 0.07	39.3 ± 0.07
2001	21.4 ± 0.15	42.8 ± 0.30	21.0 ± 0.04	42.0 ± 0.08	19.2± 0.05	38.4 ± 0.10
4001	11.54 ± 0.20	46.0 ± 0.80	10.5 ± 0.08	42.0 ± 0.30	9.57± 0.08	38.3 ± 0.30

dilution factor	$[As(CH_3)O_2^-]$ 100 mM		$[Rb^+]$ 100 mM	
	Measured concentration (µM)	$[As(CH_3)O_2^-]$ (mM) [a]	Measured concentration (µM)	$[Rb^+]$ (mM)[a]
501	192.0 ± 0.60	96.0 ± 0.30	191.6 ± 0.75	96.0 ± 0.40
1001	98.1 ± 0.36	98.0 ± 0.36	95.8 ± 0.90	96.0 ± 0.70
2001	48.5 ± 0.02	97.0 ± 0.04	47.3 ± 0.50	94.6 ± 0.60
4001	24.0 ± 0.03	96.0 ± 0.12	24.3 ± 0.13	97.4 ± 0.50

[a] Concentrations determined by multiplying measured concentrations by the dilution factor.

Table S3: Experimentally determined preferential interaction coefficients for NaX around *24bp*

C [M]	NaO$_2$As(CH$_3$)$_2$ Γ_{Na^+}	NaO$_2$As(CH$_3$)$_2$ Γ_{Cac^-}	NaF Γ_{Na^+}	NaClO$_4$ Γ_{Na^+}	NaCl Γ_{Na^+}	NaBr Γ_{Na^+}	NaBr Γ_{Br^-}	NaI Γ_{Na^+}
0.010	37.7 ± 0.2	-7.0 ± 0.7	37.0 ± 1.3	37.0 ± 0.9	37.0 ± 0.9	37.0 ± 0.9	-9.0 ±0.9	37.0 ± 1.0
0.050	36.9 ± 1.2	-8.4 ± 1.0	37.0 ± 1.3	36.6 ± 0.6	37.0 ± 0.7	36.0 ± 0.7	-8.7 ± 0.7	35.0 ± 1.0
0.100	36.6 ± 1.2	-9.0 ± 2.0	36.0 ± 1.0	35.6 ± 1.0	36.0 ± 1.0	35.0 ± 1.0	-10 ± 1.0	33.0 ± 1.6
0.200	36.0 ± 0.6	-9.5 ± 1.7	34.6 ± 1.5	33.7 ± 1.5	32.5 ± 1.5	32.0 ± 1.5	-14.5 ± 1.5	28.5 ±1.0
0.350	-	-	34.0 ± 1.0	32.0 ± 1.0	29.0 ± 1.5	28.0 ± 1.5	-16.7 ± 1.2	24.5 ± 1.2
0.500	34 ± 1.0	-12 ± 1.5	33.0 ± 1.2	30.0 ± 1.5	26.0 ± 1.0	24.6 ± 1.0	-21.5 ± 1.5	21.5 ± 1.4

Table S4: Experimentally determined preferential interaction coefficients for RbX around *24bp*

C [M]	RbO$_2$As(CH$_3$)$_2$ Γ_{Rb^+}	RbO$_2$As(CH$_3$)$_2$ Γ_{Cac^-}	C [M]	RbF Γ_{Rb^+}	RbCl Γ_{Rb^+}	RbBr Γ_{Rb^+}	RbBr Γ_{Br^-}	RI Γ_{Rb^+}
0.015	37.0 ± 0.5	-8.5 ± 1.0	0.01	37.0 ± 1.3	36.6 ± 0.9	36.6 ± 0.4	-10.0 ±1.0	37.0 ± 0.2
0.035	37.0 ± 1.0	-9.0 ± 1.5	0.05	37.0 ± 0.5	37.2 ± 0.7	37.0 ± 0.4	-9.0± 1.5	36.5 ± 1.2
0.140	33.0 ± 0.5	-12.0 ± 1.2	0.10	35.2 ± 1.5	35.6 ± 1.5	36.1 ± 1.3	-9.8 ± 1.0	36.0 ± 1.0
0.200	32.0 ± 1.9	-15.0 ± 2.3	0.2	31.6 ± 1.4	34.3 ± 1.4	34.6 ± 1.0	-11.0 ± 1.2	34.5 ±1.2
0.300	29.0 ± 1.2	-16.7± 1.2	0.3	28.7 ± 1.7	33.0 ± 1.1	33.7 ± 0.5	-13.0± 1.2	33.5 ± 1.0
0.500	25.0 ± 1.2	-22.0 ± 1.5	0.5	24.8± 2.0	32.0 ± 1.9	32.7 ± 2.0	-15.0 ± 2	32.5 ± 1.5

Table S5: Experimentally determined preferential interaction coefficients for CsX around *24bp*

C [M]	CsF Γ_{Cs^+}	C [M]	CsBr Γ_{Cs^+}	CsBr Γ_{Br^-}
0.010	36.0 ± 1.0	0.010	37.0 ± 0.5	-8.0 ±0.5
0.018	36.0 ± 0.5	0.018	37.0 ± 0.5	-10± 1.0
0.045	35.0 ± 0.5	0.045	37.0 ± 1.0	-10.5 ± 1.0
0.090	34.0 ± 0.8	0.100	37.2 ± 1.2	-9.7 ± 1.5
0.180	30.0 ± 0.8	0.200	36.6 ± 1.0	-10.8± 1.2
0.460	22.4 ± 2.0	0.500	34.0 ± 1.8	-13.4 ± 1.8

Table S6: Comparison of preferential interactions coefficients determined herein and in previous ion counting publications.

C [M]	Γ_{Na^+}	Γ_{Cac^-}	Γ_{Na^+}	Γ_{Cac^-}	Γ_{Rb^+}	Γ_{Rb^+}
	NaO$_2$As(CH$_3$)$_2$[a]		NaO$_2$As(CH$_3$)$_2$[b]		RbCl[a]	RbCl[c]
0.010	37.7 ± 0.2	-7.0 ± 0.7	39.5 ± 2.8	-6.6 ± 1.7	36.6 ± 0.9	
0.050	36.9 ± 1.2	-8.4 ± 1.0	39.2 ± 3.0	-7.85 ± 3.0	37.2 ± 0.7	
0.100	36.6 ± 1.2	-9.0 ± 2.0	37.8 ± 2.6	-9.2 ± 1.2	35.6 ± 1.5	36 ± 1.0
0.200	36.0 ± 0.6	-9.5 ± 1.7	37.0 ± 2	-10.0 ± 1.6	34.3 ± 1.4	
0.500	34.0 ± 1.0	-12.0 ± 1.5	37.0 ± 2.0	-8.6 ± 2.5	32.0 ± 1.9	

[a] Preferential interaction coefficients determined herein.

[b] Preferential interaction coefficients provided in ref [9].

[c] Preferential interaction coefficients provided in ref [14].

Table S7. Kinetic and thermodynamic parameter for P4-P6 RNA folding

	k_{fold}[a] [s^{-1}]	k_{unfold}[a] [s^{-1}]	K_{eq}[b]	$K_{eq,bulk}$[c]	N[d]
NaF	4.4 ± 0.30	4.5 ± 0.15	0.54 ± 0.05	1.0	109
NaCl	6.4 ± 0.40	4.2 ± 0.20	1.37 ± 0.10	1.9	272
NaBr	8.5 ± 0.40	4.3 ± 0.30	1.54 ± 0.13	2.9	215
RbF	2.1 ± 0.10	2.9 ± 1.40	0.73 ± 0.05	0.9	359
RbCl	1.0 ± 0.05	5.12 ± 0.25	0.19 ± 0.01	0.3	311
RbBr	1.0 ± 0.05	5.12 ± 0.26	0.18 ± 0.01	0.3	306

a) Mean and error are bootstrap-estimated 95% confidence intervals of the mean.

b) $K_{eq} = \dfrac{k_{fold}}{k_{unfold}}$

c) $K_{eq, bulk}$ determined through a fit of the total FRET distribution of a population of molecules to two-Gaussians (Figure S6 and S7) and taken as the ration of the total time spent in the high FRET sate relative to the low FRET state.

d) N = number of molecules.

References:

(1)   Chausseau, M.; Poussel, E.; Mermet, J. M. *Spectrochim Acta B* **2000**, *55*, 1315.
(2)   Robinson, R. A.; Stokes, R. H. *Electrolyte solutions*; 2nd rev. ed.; Dover Publications: Mineola, NY, 2002.
(3)   Barthel, J.; Krienke, H.; Kunz, W. *Physical Chemistry of Electrolyte Solutions: Modern Aspects*; Steinkopf ; Springer: Darmstadt, New York, 1998.

(4)   Kunz, W. *Specific Ion Effects*; World Scientific: Singapore ; Hackensack, NJ, 2010.
(5)   Marcus, Y.; Hefter, G. *Chem Rev* **2006**, *106*, 4585.

(6)   Hamer, W. J.; Wu, Y. *J Phys Chem Ref Data* **1972**, *1*, 52.
(7)   Sharp, K. A.; Friedman, R. A.; Misra, V.; Hecht, J.; Honig, B. *Biopolymers* **1995**, *36*, 245.
(8)   Misra, V. K.; Draper, D. E. *J Mol Biol* **1999**, *294*, 1135.
(9)   Bai, Y.; Greenfeld, M.; Travers, K. J.; Chu, V. B.; Lipfert, J.; Doniach, S.; Herschlag, D. *J Am Chem Soc* **2007**, *129*, 14981.
(10)   Grochowski, P.; Trylska, J. *Biopolymers* **2008**, *89*, 93.
(11)   Harris, R. C.; Boschitsch, A. H.; Fenley, M. O. *J Chem Phys* **2014**, *140*, 075102.
(12)   Ni, H. H.; Anderson, C. F.; Record, M. T. *J Phys Chem B* **1999**, *103*, 3489.
(13)   Mills, P.; Anderson, C. F.; Record, M. T. *Biophys J* **1986**, *49*, A301.
(14)   Andresen, K.; Qiu, X. Y.; Pabit, S. A.; Lamb, J. S.; Park, H. Y.; Kwok, L. W.; Pollack, L. *Biophys J* **2008**, *95*, 287.